Available online at www.sciencedirect.com
SCIENCE DIRECT®
C. R. Physique 6 (2005) 1118–1128
COMPTES RENDUS PHYSIQUE
http://france.elsevier.com/direct/COMREN/

MCAO for very large telescopes/OAMC pour les très grands télescopes

MAD: practical implementation of MCAO concepts

Enrico Marchetti [a,*], Roland Brast [a], Bernard Delabre [a], Rob Donaldson [a], Enrico Fedrigo [a], Christoph Frank [a], Norbert Hubin [a], Johann Kolb [a], Miska Le Louarn [a], Jean-Louis Lizon [a], Sylvain Oberti [a], Fernando Quirós-Pacheco [a], Roland Reiss [a], Joana Santos [a], Sebastien Tordo [a], Elise Vernet [a], Roberto Ragazzoni [b], Carmelo Arcidiacono [b], Paolo Bagnara [c], Andrea Baruffolo [c], Emiliano Diolaiti [d], Jacopo Farinato [b], Matteo Lombini [b]

[a] *European Southern Observatory, Karl-Schwarzschild-Str. 2, 85748 Garching bei München, Germany*
[b] *INAF, Astrophysical Observatory of Arcetri, Largo Enrico Fermi 5, 50125, Florence, Italy*
[c] *INAF, Astronomical Observatory of Padova, Vicolo dell'Osservatorio 5, 35122, Padova, Italy*
[d] *INAF, Astronomical Observatory of Bologna, Via Ranzani 1, 40127, Bologna, Italy*

Abstract

The European Southern Observatory (ESO) together with external research institutes have built a Multi-Conjugate Adaptive Optics (MCAO) Demonstrator (MAD) to perform wide field-of-view adaptive optics correction (2′ in K band). The aim of MAD is to demonstrate the on-sky feasibility of the MCAO technique and to evaluate its critical aspects in the framework of both the 2nd generation instrumentation for the Very Large Telescope (VLT) and the Overwhelmingly Large Telescope (OWL). The MAD module will be installed on the VLT to perform on-sky observations. MAD comprises two deformable mirrors and two different multi-reference wavefront sensors with natural guide stars. In this article we present the MAD design, some aspects of the MAD calibration and the first closed-loop results in the laboratory in Single Conjugated Adaptive Optics (SCAO) and Ground Layer Adaptive Optics (GLAO) configurations. ***To cite this article: E. Marchetti et al., C. R. Physique 6 (2005).***

Résumé

MAD : implementation pratique de concepts en OAMC. L'ESO ainsi que des instituts de recherche externes ont développé MAD (le Démonstrateur d'Optique Adaptative Multi-Conjuguée) pour effectuer la correction d'optique adaptative grand champ (2′ en bande K). Le but de MAD est de démontrer sur le ciel la faisabilité de la technique d'OAMC et d'évaluer ses points critiques pour l'instrumentation de 2eme génération pour le VLT et pour le télescope OWL. MAD sera installé au VLT pour effectuer des observations sur le ciel. MAD utilise deux miroirs deformables et deux senseurs de front d'onde multi-référence avec des étoiles-guide naturelles. Dans cet article nous présentons la conception du démonstrateur, quelques aspects de l'étalonnage de MAD et les premiers résultats en boucle fermée dans les configurations mono-conjugée (SCAO) et correction de la couche au sol (GLAO). ***Pour citer cet article : E. Marchetti et al., C. R. Physique 6 (2005).***

* Corresponding author.
E-mail address: emarchet@eso.org (E. Marchetti).

1631-0705/$ – see front matter
doi:10.1016/j.crhy.2005.11.002

Keywords: Multi-Conjugate Adaptive Optics; Wavefront sensors; Layer oriented; Ground Layer Adaptive Optics

Mots-clés : Optique Adaptative Multi-Conjugée ; Senseurs de Front d'Onde

1. Introduction

Multi-Conjugate Adaptive Optics (MCAO) [1–3] aims at performing wide field of view atmospheric turbulence correction using many Guide Stars (GSs) surrounding the observed target. The light coming from the GSs is analyzed through wavefront sensors whose signals are used to reconstruct the atmospheric turbulence at the different heights which some deformable mirrors are conjugated to. Different approaches for MCAO correction have been proposed in the latest years such as the atmospheric tomography (also called Global Reconstruction) both in the zonal [4] and in the modal way [5] and the Layer Oriented one [6,7]. The modal tomography has been also experimentally verified on the sky [8]. These two approaches, in their basic concept, need different wavefront sensors (WFSs) concepts in order to better optimize the appropriate atmospheric reconstruction.

The European Southern Observatory in collaboration with external research institutes have built an instrument prototype, the MCAO demonstrator [9], to prove on the sky the feasibility of the MCAO technique using both reconstruction approaches in view of the future 2nd generation of the VLT instrumentation and the 100-meters telescope OWL [10]. In particular, MAD is seen as a crucial enabling milestone for OWL. MAD will be installed at the Nasmyth focus of a VLT unit telescope and the actual timeline foresees to have the on-sky operations in 2006 using only natural guide stars (NGSs).

As an intermediate step we will implement also Ground Layer AO (GLAO) correction where the signal coming from the WFSs is used to apply correction only with the ground conjugated DM. This kind of correction will provide only seeing reduction across the FoV but it will increase the encircled energy with a consequent enhancement of the signal-to-noise ratio in the detection of faint objects.

The first part of this article is dedicated to the description of the MAD system and its main components including the turbulence generator and the infrared camera, then we will focus on some aspects related to the system calibration which are common to MCAO systems, and finally the first light results of closed loop in Single Conjugate AO (SCAO) and GLAO configurations are briefly described.

2. MAD design

MAD is a prototype MCAO system performing wide Field of View (FoV) Adaptive Optics (AO) correction over 2 arcmin on the sky in K band by using bright ($m_V < 14$) Natural Guide Stars (NGS). It is implemented using existing technology and re-using as much as possible key components developed in the scope of existing AO systems.

MAD will be used to investigate two different approaches of MCAO correction with two independent wavefront sensing techniques: the Star Oriented MCAO with 3 Shack–Hartmann wavefront sensors (SHWFS) sensing simultaneously 3 NGS and the Layer Oriented MCAO with a Layer Oriented Wavefront Sensor (LOWFS) based on a Multi-Pyramid WFS [11], sensing simultaneously 8 NGS. The MAD Real-Time computer architecture is designed in order to support both reconstruction approaches.

The MAD correction is based on two deformable mirrors (DM). One mirror is conjugated to the telescope pupil for ground layer turbulence correction, the second is conjugated at 8.5 km above the telescope aperture, enabling a larger FoV correction. The MAD MCAO correction is optimized for the K (2.2 μm) band for the median Paranal seeing conditions and the performance will be evaluated at this wavelength.

For testing and tuning the MAD system in the laboratory the multi-layer turbulence generator MAPS (Multi-Atmospheric Phase screens and Stars) is placed at the MAD input focus. MAD uses the 1 arcmin FoV infrared camera CAMCAO (CAmera for MCAO) to evaluate the correction performance in K band.

2.1. Optical layout

The optical design of MAD is provided in Fig. 1. The MAD input beam is F/15. A 2 arcmin FoV is de-rotated by an optical derotator and collimated by a doublet lens to re-image a telescope pupil of 60 mm in diameter. A 100 mm DM is conjugated at an altitude of 8.5 km (DM-2) and a 60 mm DM is conjugated to the re-imaged telescope pupil (DM-1). A Tip-Tilt Mount (TTM) is supporting the DM-1 for the tip-tilt correction. A dichroic transmits the Infrared (IR) light (1–2.5 μm) towards the IR camera and reflects the visible light (0.45–0.95 μm) towards the Wavefront Sensor (WFS) path. A lens objective provides a telecentric F/20 input beam to the wavefront sensors. Two insertable folding mirrors (WFS selector) fold the light either downward to the SHWFS or upward to the LOWFS. The two WFSs are not used simultaneously.

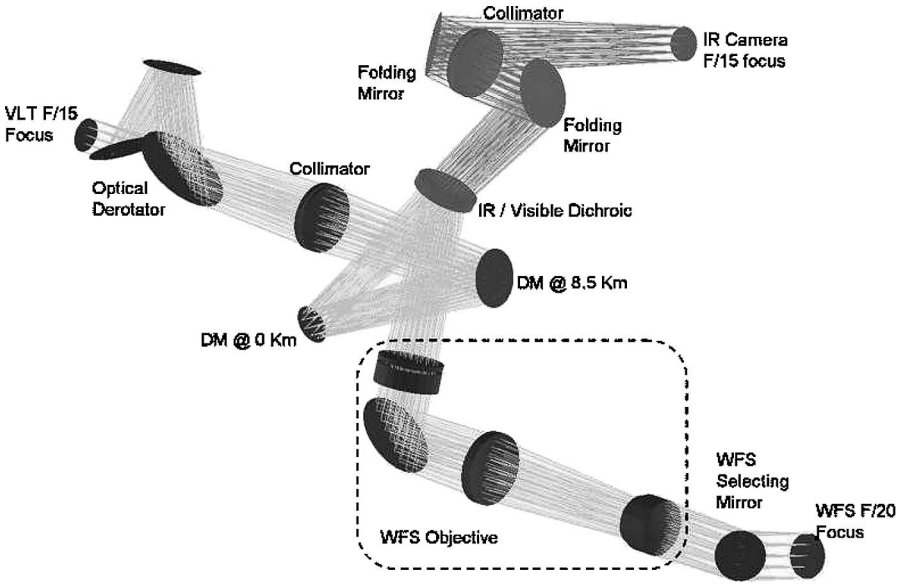

Fig. 1. MAD optical layout.

The IR beam after passing through the dichroic is folded by a mirror and then focused by a second collimator (copy of the first one) to form an F/15 focus at the entrance of the IR camera. A second folding mirror is provided to direct the focused beam perpendicularly through the bench. The IR camera, located below the bench, is interfaced with an XY table for scanning the full 2 arcmin FoV.

The turbulence generator MAPS is located in proximity of the input F/15 to inject the turbulence inside the optical train. Two AO calibration units are implemented: one at F/15 input focus (Calibration Unit 1) and one at the input of the WFS optical path (Calibration Unit 2). These units consist of a set of illuminated fibers mounted on a XY table to scan the full 2 arcmin FoV.

2.2. Wavefront sensors

2.2.1. Multi SHWFS

The Multi SHWFS consists of 3 Shack–Hartmann units (SHU) capable to scan the whole 2 arcmin FoV to pick up the NGSs for the wavefront sensing (see Fig. 2 left). Each SHU is provided with an arm supporting a pick-up mirror folding the light through the SHU optics, a FoV diaphragm of 2.4 arcsec located at the F/20 focus and doublet lenses that re-image the telescope pupil on the lenslet array. The lenslet array is an 8×8 sub-apertures, 192 μm pitch, 3.2 mm focal length. Each small lens focuses the NGS light on the WFS camera detector over 8×8 pixels, 24 μm size (scale 0.3 arcsec/pixel). Each SHU is mounted on a XY motion scanning the 2 arcmin FoV and the three arms are slightly displaced in altitude with respect to the table plane in order to avoid mutual collisions.

2.2.2. LOWFS

The LOWFS (see Fig. 2 right) is based on a multi pyramid WFS with eight pyramids to observe simultaneously eight NGSs. Even if the FoV of MAD is rather small for finding 8 bright NGSs we carefully selected asterisms on the sky which contain such a number of them. In the framework of future GLAO/MCAO systems using only NGSs it is important to demonstrate that acquiring several GSs simultaneously is feasible. Obviously, for having significant sky coverage the future systems should observe on a larger FoV in order to acquire enough GSs, even faint ones, to guarantee a reasonable correction performance. Each pyramid is supported by a small cylinder containing some re-imaging optics to enlarge the system focal ratio by a factor $\sim$10 on the top of the pyramid. The light modulated by the pyramid is then re-imaged through two groups of lenses and the pupil image of the observed NGS is created on the plane where the WFS camera detectors are located. Between the two groups of lenses a dichroic splits the light toward the two WFS cameras which are slightly displaced along the optical axis in order to provide the footprint geometries corresponding to the conjugation altitudes of the two DMs of MAD.

2.2.3. Detector system

The MAD detector system consists of 5 WFS cameras (3 for the SHWFS and 2 for the LOWFS) based on the E2V CCD39 chip, having 80×80 pixel (24 μm) and 4 outputs. Each CCD39 chip is included in a Peltier cooler and mounted inside a small

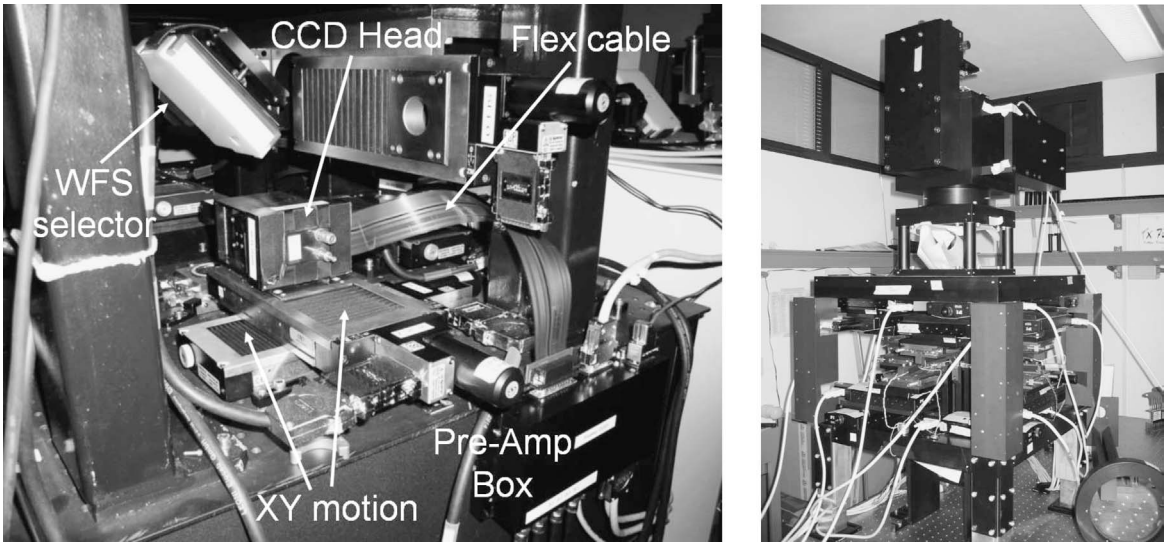

Fig. 2. Left: Multi SHWFS, here is shown only one of the three units. Right: LOWFS, the pyramids are located in the lower part of the WFS and the detector are located in the upper one.

compact head. The CCDs have a flexible cable for connecting with the pre-amplifiers allowing easy translation of the full CCD head.

The CCD39 chips are controlled by a FIERA system [12]. For the SHWFS 12 outputs will be used simultaneously, for the LOWFS only 8 outputs. For the SHWFS, FIERA will be able to drive the detectors simultaneously at the same frame rate while for the LOWFS it is required to run the two detectors at different frame rates. The maximum frame rate required is 400 Hz. FIERA will not drive the two WFS at the same time.

In the SHWFS the useful surface of the detectors is divided into 8×8 sub-apertures, 8×8 pixels each. The number of useful sub-apertures is 52. In the LOWFS the detector conjugated with the ground layer has a fixed binning of 2×2 while the detector conjugated to 8.5 km has a fixed binning of 4×4. Taking into account the difference of the footprint size of the 2 arcmin FoV at the two altitudes, for the ground conjugated detector the resulting sub-aperture grid is 8×8, while for the high altitude conjugated one is 7×7.

2.3. Deformable mirrors

The Deformable Mirror conjugated to the ground is the MACAO SINFONI [13] bimorph DM, 60 actuators, 60 mm pupil, radial geometry (see Fig. 3). The Deformable Mirror conjugated to the altitude of 8.5 km is the MACAO-VLTI [14] bimorph DM, 60 actuators, 100 mm pupil, radial geometry (see Fig. 3). The tip-tilt correction is provided by the SINFONI Tip-Tilt supporting the MACAO SINFONI DM.

2.4. Real-time computer

The MAD Real-Time Computer [15] has been designed to support both the Star Oriented and the Layer Oriented wavefront sensing techniques and to implement both the Global and the Local Reconstruction. Even if the Global Reconstruction is proper of the Star Oriented mode and the Local Reconstruction is proper of the Layer Oriented mode these WFS techniques can be mutually exchanged with respect to the reconstruction approaches by combining numerically (Star Oriented) or optically (Layer Oriented) the light of the sensed NGSs.

The MAD Real-Time Computer (RTC) subsystem is organized in three nested control loops. The primary loop, which is the main loop, where the atmospheric wavefront is compensated. It goes from the wavefront sensors to the deformable mirrors and it runs at 400 Hz. The secondary loop, where a portion of the tip-tilt component compensated by the DMs is off-loaded at each cycle to the TTM (5 Hz). The tertiary loop where the TTM is out of stroke for slow large movements: the control loop computes this slow drift and it makes it available to the MAD Observing Software to compensate for it (0.2 Hz) through the VLT Active Optics system.

In the MAD RTC Hardware architecture a standard ESO instrument workstation (WS) is used to interface to the Local Control Unit (LCU) and hosting the WS components of the MAD RTC software. The supervisory Computer (LCU) is

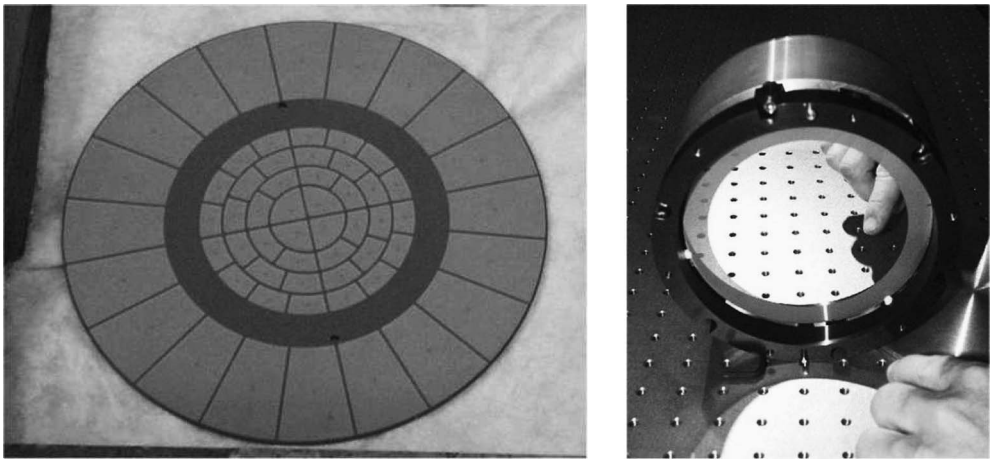

Fig. 3. Left: Geometry of the actuators in the MAD deformable mirrors. Right: MACAO VLTI DM.

a PowerPC (PPC) 604 mountable in a VME rack. It has a RS232 serial link going to the High Voltage Amplifier for housekeeping operations. The RTC is the Dy4 CHAMP-AV board, a Quad-G4 board that mounts 4 PowerPC 7410 running at 500 MHz. The connection between the Real-Time Computer and FIERA is assured by a 32 bit digital I/O board.

2.5. Turbulence generator MAPS

The MAPS [16] goal is to emulate a time evolving three-dimensional atmosphere whose induced aberrations are injected into MAD. The characteristics of the atmospheric turbulence will be similar to those of the Paranal observatory during median seeing conditions (seeing $= 0.73''$, $\tau_0 = 3.4$ ms, $\theta_0 = 2.2''$, $L_0 = 22$ m). The evolving atmosphere is reproduced by three rotating transmissive plates, called Phase Screens (PS). The surface of the plate is chemically etched in order to create a spatially varying thickness which causes a phase shift in a wavefront passing through it.

A view of MAPS is shown in Fig. 4. The Natural Guide Stars (NGS) are emulated by up to 34 visible-IR light transmissive fibers. The fiber positions will be changeable to create the desired star configuration in a FoV of 2 arcmin. A first group of lenses collimates the light beams from the NGSs and allows the telescope pupil to be created. Three PSs are located in the collimated beams to emulate the atmospheric layers at 0, 6 and 8.5 km. The PSs have different turbulence power according to the expected vertical distribution. The evolving atmosphere is emulated by rotating the PSs at different speeds according to the wind speed vertical profile. The position of the 8.5 km PS can be varied up to 13 km in order to modify the atmospheric

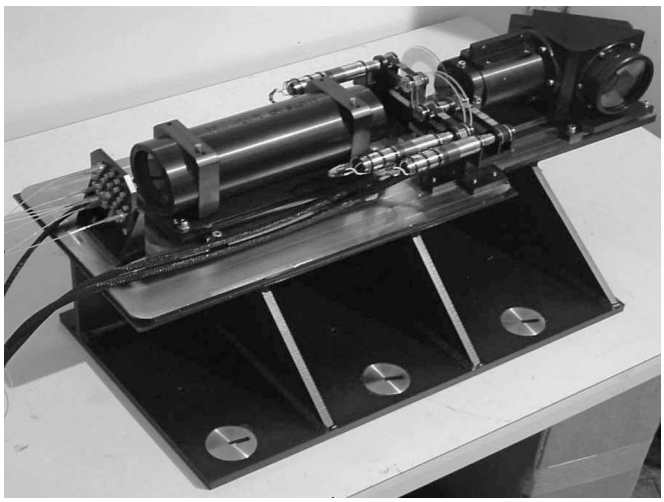

Fig. 4. The turbulence generator MAPS. It is installed at the MAD input F/15 focus.

anisoplanatism. The rotating speeds can be adjusted to reproduce a wide range of atmospheric correlation times. Moreover the PSs are interchangeable in order to emulate a selected range of seeing conditions.

A second group of lenses re-images the artificial NGSs whose wavefronts are deformated by the PSs. The distorted wavefronts are then injected into MAD for GL-MC/AO correction.

2.6. Infrared camera CAMCAO

The CAMCAO IR camera [17] is a 1 arcmin FoV camera with pixel scale of 0.028 arcsec/pixel (Nyquist sampling in K band). CAMCAO is used to evaluate the wide FoV GL-MC/AO correction of MAD. CAMCAO is based on a $2k \times 2k$ Hawaii2 IR detector controlled by a standard IRACE system [18].

The camera will have standard IR band filters mounted on a manually positionable filter wheel. CAMCAO is placed in F/15 beam after the dichroic and it is provided with a cooled optical system, based only on spherical mirrors with field and pupil cold stops. In order to optimize the IR detector performance, different cooling systems allowing temperatures lower than liquid Nitrogen (baseline cooling for CAMCAO) have been considered. The possible use of Close Cycle cooling or Pulse tube systems is under investigation.

3. Static aberrations calibration

The calibration of the static aberration in the infrared (IR) path of an AO system is a critical issue. In fact the WFS and the IR path normally differ in terms of optical aberrations and a careful characterization of these noncommon path aberration should be implemented in order to optimize the image quality at the IR camera focus. As a general rule the best static image is the one with the highest Strehl at any IR band (no turbulence). It is possible to retrieve the wavefront aberrations in the IR path and then correct them by applying a static offset at the DM surface. The slope offsets at the level of the SHWFS sub-apertures will be measured after applying the DM static offset and the AO loop will be closed around these slope offsets.

In MAD we measured the static aberrations in the IR path using the Phase Diversity method [19,20]: the wavefront aberrating a point source image is retrieved by comparing an in-focus image with a slightly defocussed image of the source. The process is implemented iteratively by applying to the DM the correction computed at the previous step. We introduce a variation to the standard Phase Diversity method: we still use a modal reconstruction (Zernike polynomials) of the wavefront but we record the modal deformations to the DM by introducing the corresponding slope offsets in the SHWFS and closing the loop around them. This technique guarantees a better stability of the measurements and increases the sensitivity of the method. In Fig. 5 is shown the correction achieved on axis with Phase Diversity on MAD.

In MAD we plan to extend the static aberration correction in MCAO fashion by measuring the static wavefront at different positions of the FoV and then, by tomographic reconstruction, optimize for the highest and flattest Strehl applying a static offset to the DMs conjugated at different altitudes.

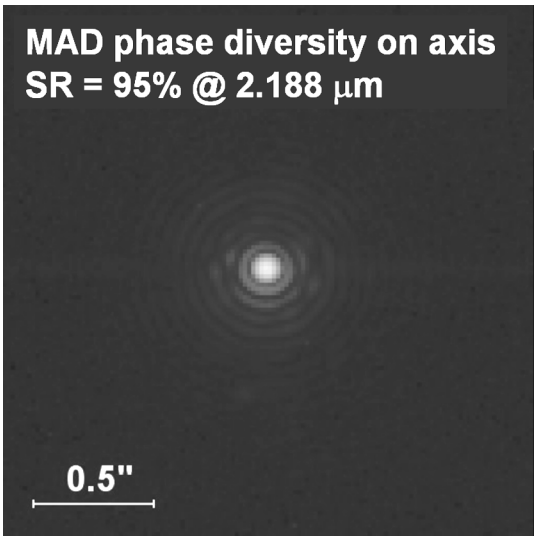

Fig. 5. On axis image of single mode fiber after Phase Diversity correction without turbulence.

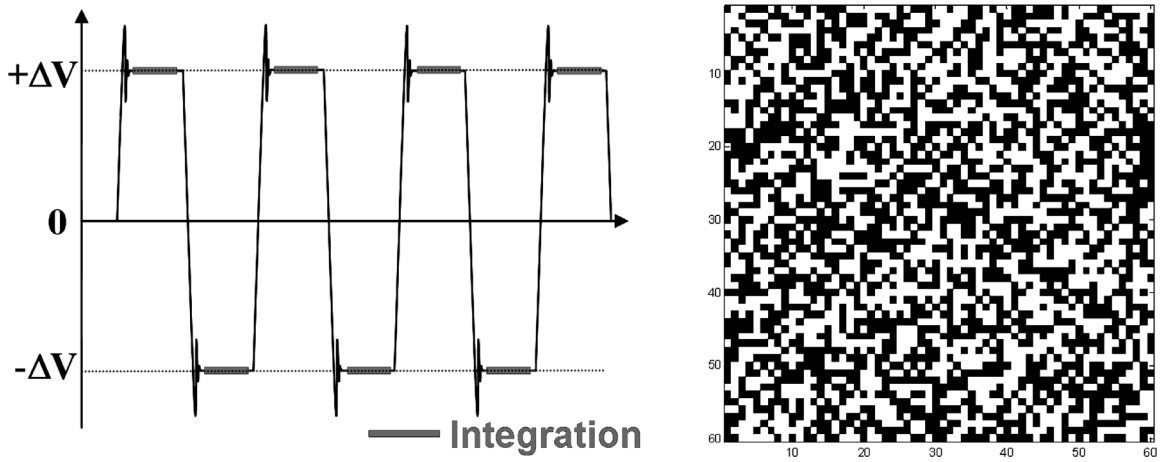

Fig. 6. Left: The integration for the IM recording is applied when the actuator is pushed and pulled and skipping the overshoot phase. Right: Hadamard matrix of order 60.

4. Interaction matrix calibration

The calibration of the Interaction Matrix (IM) is one of the most critical aspects involving the operations of an AO system. The IM matrix can be considered as the core of the system characterization because it represents the physical link between the WFSs and the DMs. It must be carefully calibrated taking into account the specificity of each different subsystem.

In MAD, as in other AO systems, the IM is affected by the limited range of WFS's linearity, the creep of the DM, the hysteresis and the non-linearity of the actuator response and the resonances of the DM. Moreover the internal turbulence and the limited Signal to Noise Ratio (SNR) of the measurements bring additional disturbance when recording the IM. In MAD we record the IM by fast actuation of the DM by pushing and pulling the actuators and to freeze the creep and the internal turbulence by subtracting the two signals. The first few steps after each actuation are skipped in order to avoid the actuator overshooting (see Fig. 6 left).

A further step in optimizing both the SNR and the speed of the IM recording (typically long in an MCAO system because of the several WFSs and DMs) we benefit from the use of the Hadamard matrices [21]. The Hadamard matrix of order n is a $n \times n$ square matrix which entries are either $+1$ or -1 and satisfies the property $H \cdot H^T = nI_n$ where I_n is the $n \times n$ identity matrix. Instead of pushing–pulling an actuator per time it is possible to push–pull all the actuators simultaneously with a pattern given by a row of a Hadamard matrix. The multiple actuation will be repeated for all the rows of the Hadamard matrix and the slopes recorded are then multiplied by the transpose of it. The time spent in this process is the same used in the single actuation case but the SNR will be n times larger. Fig. 6 right shows a Hadamard matrix of order 60 (DM actuators number) used for the MAD SCAO calibration with a SHWFS. In the MCAO IM calibration we will use a Hadamard matrix of order 120.

5. MAD reconstruction and control

For the Star Oriented mode of MAD we plan to implement different reconstruction and control approaches for SCAO, GLAO and MCAO operations.

The simplest will be the Least Square reconstructor (LS), using the generalized inverse of the IM with truncation of badly sensed modes:

$$R_{\mathrm{LS}} = (M_{\mathrm{int}}^T \cdot M_{\mathrm{int}})^{-1} \cdot M_{\mathrm{int}}^T$$

where M_{int} is the IM. In Fig. 7 is shown the MAD SCAO IM obtained with a SHWFS (left) and the condition number of the IM as a function of the system modes (right): the last mode corresponds to the piston and just removing it the condition number drops from 94 to 46.

Another reconstructor we will implement on MAD will be the Maximum-A-Posteriori reconstructor (MAP) which takes into account spatial a priori knowledge on the turbulence and measurement noise. It gives a better performance in the whole FoV as it can properly handle the badly-seen modes that typically show up in MCAO systems:

$$R_{\mathrm{MAP}} = C_\varphi \cdot M_{\mathrm{int}}^T \cdot (M_{\mathrm{int}} \cdot C_\varphi \cdot M_{\mathrm{int}}^T + C_b)^{-1}$$

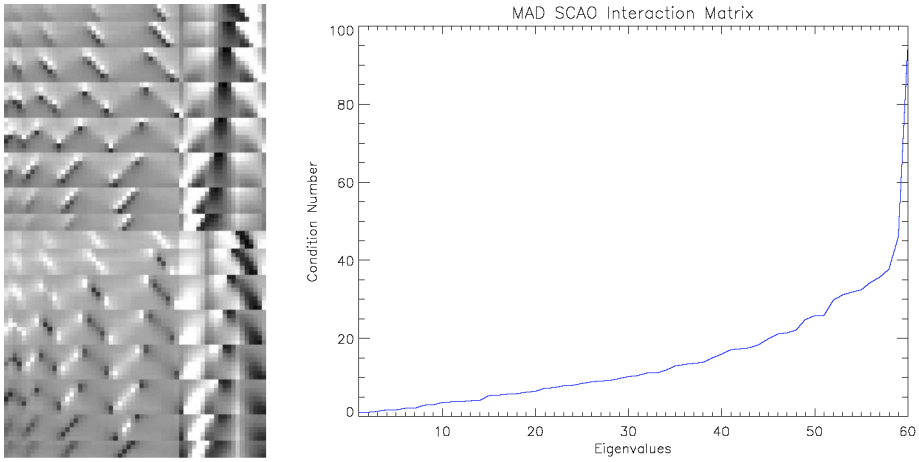

Fig. 7. Left: The MAD Interaction Matrix obtained for one SHWFS and the ground conjugated DM. Right: the condition number of the IM. When filtering the last system modes (piston) the condition number drops from 98 to 46.

where C_φ is the covariance matrix of the turbulence projected onto the modes used in the reconstruction and C_b is the noise covariance matrix. However, since C_φ does not correspond to the statistics of the residuals after closed-loop correction, we envisage to implement an approach similar to the pseudo-open-loop control (POLC) proposed in Ref. [22] to ensure closed-loop stability.

Provisions are made also for correction on a specific portion and direction of the FoV. This reconstruction approach boosts the performance in a given direction and smaller portion of the scientific FoV giving higher correction performances. The improvement in correction at this specified direction is achieved at the expense of the uniformity of the correction in the whole FoV. The wavefront reconstructor is based on the minimum-variance (MV) reconstructor [23] which can be expressed as the product of two matrices:

$$R_{\mathrm{MV}} = P \cdot E$$

The matrix E represents a full tomographic reconstruction of the turbulence volume (possible only when having a knowledge of the vertical distribution of the atmospheric turbulence, obtained in real time from vertical profilometer), and the matrix P stands for an optimal projection from the reconstructed turbulent layers onto the two deformable mirrors taking into account the direction(s) where optimization is desired.

The temporal control of MAD will range from a simple integrator (same gain for all controlled modes):

$$C(z) = \frac{g}{1 - z^{-1}}$$

to the Optimized Modal Gain Integrator (OMGI) customized for MCAO [24] where the gain is tuned independently for each controlled mode in order to minimize the residual variance associated to it.

At a later stage we will implement a more sophisticated control based on Kalman filtering [25].

6. First light results

Hereafter we present the first light results obtained with MAD in SCAO and GLAO configuration. It is worth noting that these results are just preliminary and do not represent the final performance of the system since the optimization process is still in progress.

6.1. Single Conjugated AO

The loop has been closed using one SHWFS and the ground conjugated DM. Only one rotating phase screen with gentle atmosphere has been used in order to facilitate the first light operations. The seeing was $0.4''$ in V band (0.5 µm) and the wind speed was set to 10 m/s. The loop was closed at a frequency of 115 Hz on a $m_V = 6$ star and a Strehl of 52% in K band has been obtained. Fig. 8 shows the open- and closed-loop images taken in K band. The cross-shaped artefact in the closed-loop image is due to a non-perfect filtering of some badly seen system modes.

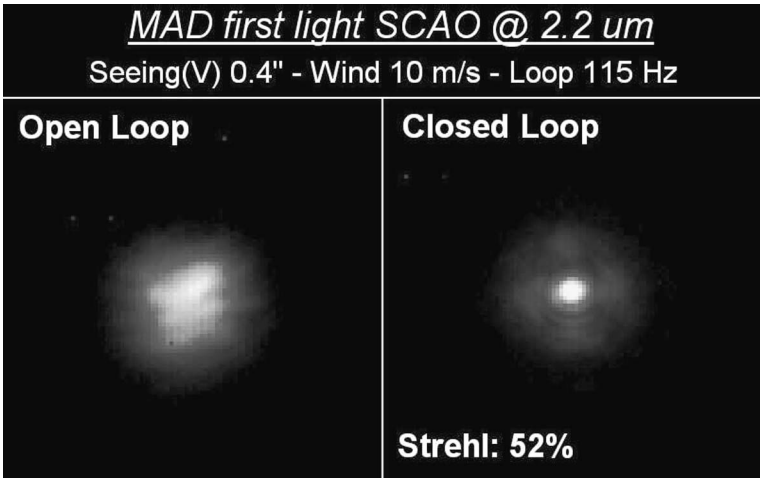

Fig. 8. First light closed loop in SCAO configuration.

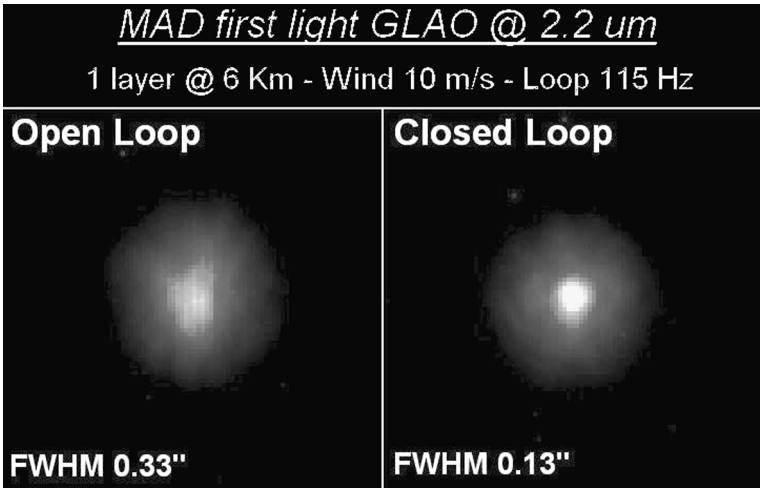

Fig. 9. MAD first light Ground Layer AO closed loop. Only one phase screen at 6 km altitude have been used and the guide stars were located on a circle of 1.5 arcmin diameter. The FWHM reduction factor is ∼2.5.

6.2. Ground Layer AO

The loop has been closed using three SHWFS located on a circle of 1.5 arcmin at the vertex of an equilateral triangle and the correction was applied through the ground conjugated DM. Only one rotating phase screen located at 6 km altitude has been used to simulate a gentle anisoplanatism. The seeing was $0.45''$ in V band and the wind speed 10 m/s. The loop was closed at a frequency of 115 Hz on $m_V = 6$ star. The FWHM in K band has been reduced by a factor ∼2.5 demonstrating the fact that MAD is capable to perform GLAO correction (see Fig. 9). The gain in Encircled Energy is shown in Fig. 10: at the level of the FWHM of the closed-loop image the gain of energy concentration has increased by a factor ∼2.

7. Conclusions

The MAD system has been designed to perform GLAO and MCAO correction on a 2 arcmin FoV and to evaluate the performance in K band. The MAD system has been completely integrated and we have already started the closed-loop operations.

We dedicated quite some time and efforts in calibrating and characterizing carefully all the subsystems. We achieved 95% Strehl image in K band correcting for non-common-path aberration in the IR path using a closed-loop adaptation of the Phase Diversity technique.

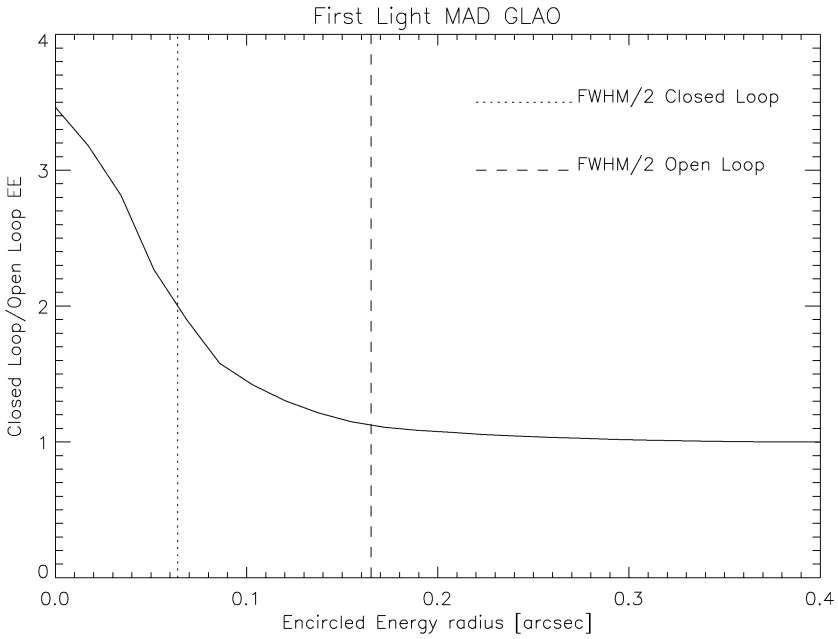

Fig. 10. Encircled Energy gain in GLAO closed loop. At the FWHM radius of the corrected image the gain is ∼2.

We carefully calibrated the IM by using fast actuation of the DM and implementing the Hadamard matrix method. This allowed us to have very good SNR in recording the IM with a significant reduction of the time spent for the calibration.

We plan to have several reconstruction techniques and temporal controllers which will be implemented during the long phase of laboratory testing at the ESO premises.

MAD had already the first light both for SCAO and GLAO configurations demonstrating the functionality of the system and giving a positive feed-back on the strategy we planned at the beginning of the project.

The next step will be to optimize both the SCAO and GLAO configurations and to proceed to the MCAO configuration. Finally MAD will be installed at VLT for the on-sky verification.

Acknowledgements

This research has benefited from the support of the European Commission RTN program: “Adaptive Optics for the Extremely Large Telescopes”, contract no. HPRN-CT-2000-00147.

References

[1] J.M. Beckers, Increasing the size of the isoplanatic patch size with multiconjugate adaptive optics, in: M.-H. Hulrich (Ed.), ESO Conference on Very Large Telescopes and Their Instrumentation, 1988, p. 693.
[2] J.M. Beckers, Detailed compensation of atmospheric seeing using multiconjugate adaptive optics, Proc. SPIE 1114 (1989) 215–217.
[3] B. Ellerbroek, First order performance evaluation of adaptive optics system for atmospheric turbulence compensation in extended field-of-view astronomical telescope, JOSA-A 11 (1994) 783–805.
[4] M. Tallon, R. Foy, Adaptive telescope with laser probe—Isoplanatism and cone effect, A&A 235 (1990) 549–557.
[5] R. Ragazzoni, E. Marchetti, F. Rigaut, Modal tomography for adaptive optics, A&A 342 (1999) L53–L56.
[6] R. Ragazzoni, Adaptive optics for giants telescopes: NGS vs. LGS, in: T. Andersen, A. Ardeberg, R. Gilmozzi (Eds.), ESO Proceedings of the Bäckaskog Workshop on Extremely Large Telescopes, vol. 57, 2000, pp. 175–180.
[7] R. Ragazzoni, J. Farinato, E. Marchetti, Adaptive optics for 100-m-class telescopes: new challenges require new solutions, Proc. SPIE 4007 (2000) 1076–1087.
[8] R. Ragazzoni, E. Marchetti, G. Valente, Adaptive-optics correction available for the whole sky, Nature 403 (2000) 54–56.
[9] E. Marchetti, R. Brast, B. Delabre, R. Donaldson, E. Fedrigo, C. Frank, N. Hubin, J. Kolb, M. Le Louarn, J.-L. Lizon, S. Oberti, R. Reiss, J. Santos, S. Tordo, R. Ragazzoni, C. Arcidiacono, A. Baruffolo, E. Diolaiti, J. Farinato, E. Vernet, MAD the ESO multi-conjugate adaptive optics demonstrator, Proc. SPIE 5490 (2004) 236–247.

[10] P. Dierickx, E. Brunetto, F. Comeron, R. Gilmozzi, F. Gonté, F. Koch, M. Le Louarn, G. Monnet, J. Spyromilio, I. Surdej, C. Verinaud, N. Yaitskova, OWL phase A status report, Proc. SPIE 5489 (2004) 391–406.
[11] R. Ragazzoni, Pupil plane wave front sensing with an oscillating prism, J. Mod. Opt. 43 (1996) 289–293.
[12] J.W. Beletic, R. Gerdes, R.C. Duvarney, Fiera: ESO's new generation CCD controller, ExA 8 (1998) 13–24.
[13] H. Bonnet, R. Conzelmann, B. Delabre, R. Donaldson, E. Fedrigo, N. Hubin, M. Kissler-Patig, J.-L. Lizon, J. Paufique, S. Rossi, S. Ströble, S. Tordo, First light of SINFONI AO-module at VLT, Proc. SPIE 5490 (2004) 130–138.
[14] R. Arsenault, R. Donaldson, C. Dupuy, E. Fedrigo, N. Hubin, L. Ivanescu, M. Kasper, S. Oberti, J. Paufique, S. Rossi, A. Silber, B. Delabre, J.-L. Lizon, P. Gigan, MACAO–VLTI adaptive optics systems performance, Proc. SPIE 5490 (2004) 47–58.
[15] E. Fedrigo, R. Donaldson, Architecture of the MAD real-time computer, Proc. SPIE 4839 (2003) 600–611.
[16] J. Kolb, E. Marchetti, S. Tisserand, F. Franza, B. Delabre, F. Gonté, R. Brast, S. Jacob, F. Reversat, MAPS, a turbulence simulator for MCAO, Proc. SPIE 5490 (2004) 794–804.
[17] A. Amorim, A. Melo, J. Alves, J. Rebordao, J. Pinhao, G. Bonfait, J. Lima, R. Barros, R. Fernandes, I. Catarino, M. Carvalho, R. Marques, J.-M. Poncet, F. Duarte Santos, G. Finger, N. Hubin, G. Huster, F. Koch, J.-L. Lizon, E. Marchetti, The CAMCAO infrared camera, Proc. SPIE 5492 (2004) 1699–1709.
[18] M. Meyer, G. Finger, H. Mehrgan, G. Nicolini, J. Stegmeier, ESO infrared detector high-speed array control and processing electronic IRACE, Proc. SPIE 3354 (1998) 134–138.
[19] A. Blanc, T. Fusco, M. Hartung, M.L. Mugnier, G. Rousset, Calibration of NAOS and CONICA static aberrations. Application of the phase diversity technique, A&A 399 (2003) 373–383.
[20] J. Kolb, E. Marchetti, G. Rousset, T. Fusco, Calibration of the static aberrations in an MCAO system, Proc. SPIE 5490 (2004) 299–308.
[21] M. Kasper, E. Fedrigo, P.D. Looze, H. Bonnet, L. Ivanescu, S. Oberti, Fast calibration of high order adaptive optics systems, JOSA 21 (2004) 1004–1008.
[22] L. Gilles, Closed-loop stability and performance analysis of least-squares and minimum-variance control algorithms for multiconjugate adaptive optics, Appl. Opt. 44 (2005) 993–1002.
[23] T. Fusco, J.M. Conan, G. Rousset, L.M. Mugnier, V. Michau, Optimal wave-front reconstruction strategies for multiconjugate adaptive optics, JOSA-A 18 (2001) 2527–2538.
[24] F. Quirós-Pacheco, C. Petit, J.M. Conan, T. Fusco, E. Marchetti, Control laws for a multi-conjugate adaptive optics system, Proc. SPIE 5490 (2004) 1460–1471.
[25] C. Petit, J.M. Conan, C. Kulcsár, H.F. Raynaud, T. Fusco, J. Montri, D. Rabaud, Optimal control for Multi-Conjugate Adaptive Optics, C. R. Physique 6 (2005), in this issue.